Title
Investigation of RNA structure in satellite panicum mosaic virus

Journal
Virology, 351(2)

ISSN
0042-6822

Authors
Makino, DL
Day, J
Larson, SB
et al.

Publication Date
2006-08-01

DOI
10.1016/j.virol.2006.03.028

Available online at www.sciencedirect.com
SCIENCE DIRECT®
Virology 351 (2006) 420–431
VIROLOGY
www.elsevier.com/locate/yviro

Investigation of RNA structure in satellite panicum mosaic virus

D.L. Makino[1], J. Day, S.B. Larson, A. McPherson *

Department of Molecular Biology and Biochemistry, University of California, Irvine, 560 Steinhaus Hall, Irvine, CA 92697-3900, USA

Received 1 February 2006; returned to author for revision 15 February 2006; accepted 6 March 2006
Available online 4 May 2006

Abstract

Three new crystal forms of satellite panicum mosaic virus (SPMV) were grown and their structures solved from X-ray diffraction data using molecular replacement techniques. The crystals were grown under conditions of pH and ionic strength that were appreciably different then those used for the original structure determination. In rhombohedral crystals grown at pH 8.5 and low ionic strength PEG 3350 solutions, Fourier syntheses revealed segments, ten amino acid residues long, of amino-terminal polypeptides not previously seen, as well as masses of electron density within concavities on the interior of the capsid, which appeared in the neighborhoods of icosahedral five- and threefold axes. The densities were compatible with secondary structural domains of RNA, and they included a segment of double helical RNA of about four to five base pairs oriented, at least approximately, along the fivefold axes. The distribution of RNA observed for SPMV appears to be distinctly different than the encapsidated nucleic acid conformation previously suggested for another satellite virus, satellite tobacco mosaic virus. This study further shows that analysis of viruses in crystals grown under different chemical conditions may reveal additional information regarding the structure of encapsidated RNA.

Keywords: Satellite panicum mosaic virus; SPMV; Plant virus; Icosahedral symmetry; RNA structure; X-ray crystallography

Introduction

Satellite panicum mosaic virus (SPMV) infects St. Augustine grass and a wide variety of other wild and domestic grasses, but only in the presence of its helper virus, panicum mosaic virus (PMV) (Francki, 1985; Scholthof, 1999). The genome of SPMV is an 826-nucleotide, positive-sense, single-stranded RNA (Masuta et al., 1987). It is known to encode only the coat protein, which has the novel property of encapsidating both SPMV RNA and satellite RNAs of PMV (Desvoyes and Scholthof, 2000). SPMV relies on enzymes coded by PMV for its replication and intercellular transport (Scholthof, 1999). The coat protein of SPMV, which is composed of 157 amino acids, has M_r = 16,965 Da (Gasteiger et al., 2005). It neither shows sequence homology to PMV nor demonstrates any serological relationship (Buzen et al., 1984; Masuta et al., 1987). The capsid displays T = 1 icosahedral symmetry and is composed of 60 identical coat protein subunits. SPMV, purified from infected millet plants, was crystallized (Day et al., 1994) and its structure solved to 1.9 Å resolution by X-ray diffraction (Ban and McPherson, 1995).

SPMV is the smallest encapsidated virus currently known. It has a mean diameter of 160 Å, with little protrusion of its twelve pentameric capsomeres from the surface of the T = 1 particle. The capsid structure of SPMV has been compared in detail with that of the two other known plant satellite viruses, satellite tobacco mosaic virus (STMV), and satellite tobacco necrosis virus (STNV), each of which has a unique structure and bears little resemblance to another (Ban et al., 1995).

A question of considerable importance is the conformation of the single-stranded RNA genomes in these satellite viruses, which may well be different in each. It is further pertinent because it reflects on the physiological properties of the viruses, including the mechanisms by which they assemble. In the case of STMV, nearly 45% of the 1058 nucleotide RNA was immediately visible in electron density maps as a series of helical stems closed by loops, the stem–loops disposed at each of the thirty icosahedral dyad axes. Much of the remainder of the RNA could be inferred from that seen directly, and this gave rise

* Corresponding author. Fax: +1 949 824 8551.
E-mail addresses: dmakino@berkeley.edu (D.L. Makino), jsday@uci.edu (J. Day), slarson@uci.edu (S.B. Larson), amcphers@uci.edu (A. McPherson).
[1] Department of Molecular and Cell Biology, University of California, Berkeley, 16 Barker MC3202, Berkeley, CA 94720-3202, USA. Fax: +1 510 643 2352.

0042-6822/$ - see front matter © 2006 Elsevier Inc. All rights reserved.
doi:10.1016/j.virol.2006.03.028

to a model for the RNA consisting of a sequential array of stem–loops arranged so that dyad axes of the helical segments were coincident with the icosahedral twofold axes of the particle (Larson and McPherson, 2001; Larson et al., 1993). In the cases of STNV and SPMV, however, no RNA was visualized by X-ray diffraction analysis, only the protein capsid (Jones and Liljas, 1984; Ban and McPherson, 1995).

It is noteworthy that for all three satellite viruses, the amino-terminal polypeptides of the coat proteins were not visible in electron density maps, implying some degree of disorder, or the existence of multiple conformations. In STMV, some of the alternate conformations of the peptide could be resolved using low-resolution Fourier maps. It was seen that the highly positively charged, 15 amino-terminal amino acids interacted in more or less nonspecific ways with the polyphosphate backbone of the RNA (Day et al., 2001). In SPMV, the unseen amino-terminal tails are 16 amino acids in length, bearing 8 positive charges (6 arginine and 1 lysine residues, plus the amino-terminus). As for STMV, also for SPMV, these are almost certain to be interacting with the encapsidated nucleic acid. A salient difference between STMV and SPMV is that in STMV, the amino-terminal polypeptides disappear into the interior of the particle near the threefold axes, whereas in SPMV they seem to plunge toward the particle center in pairs at the icosahedral twofold axes.

The original structure determination of SPMV utilized crystals grown in the presence of 35–45% saturated ammonium sulfate. These were of cubic space group $P4_232$ (Ban and McPherson, 1995). The model was refined to an R factor of 21% at 1.9 Å resolution. From a long history of investigations on small icosahedral viruses ($T = 1$ and $T = 3$ primarily), it has become evident that the internal arrangement of nucleic acid may be dependent on conditions of pH and ionic strength. Thus, we felt that there was some possibility that the conformation of the RNA in SPMV might be similarly susceptible, and that under other physical–chemical conditions, it might be better ordered, or differently disposed, and in turn be more visible in electron density maps. Indeed, additional crystal forms of SPMV had been observed under other crystallization conditions, particularly at higher pH and lower ionic strength. There is ample evidence in the literature that alterations in pH and ionic environment may significantly affect nucleic acid structure in viruses (Kaper, 1975; Day et al., 2001; Speir et al., 1995; Casjens, 1985). We therefore felt that there was a good possibility that an altered chemical environment might produce greater conformity of the encapsidated nucleic acid structure with the icosahedral symmetry of the capsid. We thus undertook a study by X-ray diffraction of some of these alternate crystal forms with the hope that we might better define the conformation of the RNA and/or that of the associated amino-terminal tails. Given the excellent starting model available to us (Ban and McPherson, 1995), the alternate crystal forms could each be addressed by molecular replacement techniques.

Results

Three new crystal forms were examined. These had unit cells of space groups R3 ($a = b = 175.47$ Å, $c = 418.29$ Å, hexagonal setting), $P2_13$ ($a = b = c = 226.35$ Å), and P4 ($a = b = 167.06$ Å, $c = 473.21$ Å). The crystals from which the structure of SPMV was originally solved and refined were of space group $P4_232$ ($a = b = c = 183.0$ Å). None of the new crystal forms diffracted to the resolution of the original form. The R3 form diffracted to about 4.6 Å resolution, the $P2_13$ unit cell to 3.3 Å, and the P4 crystals to about 4 Å. For data collection, the $P2_13$ crystals were flash frozen after glutaraldehyde fixation whereas the R3 crystals were maintained at 22 °C for data collection and were unfixed.

By comparison with the volume of the cubic unit cell of the $P4_232$ crystals (V = 2.385 $Å^3$/Da) and the number of virus particles it contained, we deduced the number of virus particles in the new unit cells. There were four virions in the $P2_13$ and P4 unit cells, and one in the primitive rhombohedral unit cell. The asymmetric unit in the P4 unit cell was an entire virion, which was unconstrained in orientation or position. In both the $P2_13$ cubic unit cell and the R3 rhombohedral cell, however, the centers of the virus particles were constrained to lie on crystallographic threefold axes, coincident with particle icosahedral threefold axes. The numbers of coat protein subunits in the asymmetric units of the three crystal forms were therefore 60 for the P4 unit cell and 20 for the $P2_13$ and R3 unit cells.

The problem of deducing the dispositions of the particles in the latter two unit cells was reduced to finding the rotation of the particles about the crystallographic threefold axis and also, for the cubic space group, to finding the position of the particle center of mass. This was complicated to some extent because, based on previous experiences (Larson et al., 2005), it could not be assumed that the radii of the particles were exactly the same at both high and low pH, high and low ionic strengths, and under cryoconditions, as were the particles in the cubic crystals used for the original structure determination (Ban and McPherson, 1995). Those crystals were grown in an unbuffered solution containing high salt concentration, and the data were collected at room temperature. Thus, translational and rotational searches had to be carried out simultaneously with incremental variation in the radii of the particles.

In the new unit cells, the orientations were best defined by the directions of the icosahedral fivefold axes. These were unambiguous in 72° kappa sections of self-rotation functions, as seen in Fig. 1. The 120° and 180° kappa sections confirmed the directions of the fivefold axes and the particle orientations. Peaks corresponding to icosahedral symmetry were clearly evident for the R3 and $P2_13$ unit cells, but not for the P4 crystal, which was deemed not worthy of further pursuit.

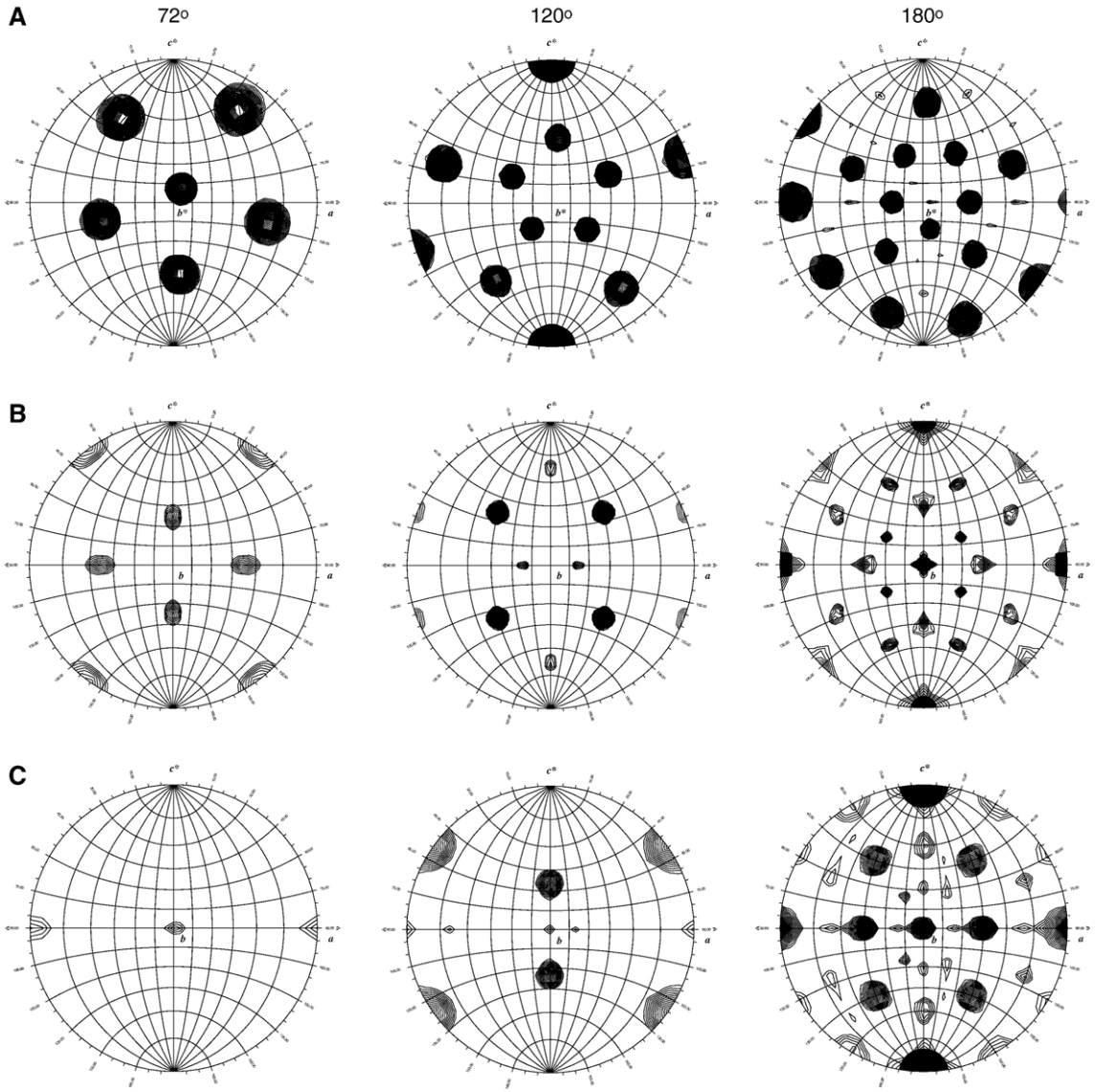

Fig. 1. Self-rotation function diagrams showing kappa sections corresponding to the five-, three-, and twofold symmetry axes in the (a) R3, (b) $P2_13$, and (c) P4 crystals. Reflections within the range 20–4.6 Å and above 2.0 sigma were used in the calculation. View is along the *y* axis. Polar angle psi is shown on the perimeter of the circle, and the phi angle is on the equatorial line.

Because space group R3 has an arbitrary origin along the threefold axis, only the center of the virus particle in the $P2_13$ unit cell had to be determined. The center of mass of the particle in the cubic unit cell was incrementally translated along the body diagonal of the cell over a range limited by packing considerations, and the correlation coefficient evaluated at each point as a function of the particle radius. The radius was varied over a range of minus 10 to plus 10 Å. When the optimum particle center and radius were found, the appropriate skew matrix defining the dispositions of all protein subunits in the asymmetric unit was calculated. This was followed by a repetitive process of refinement and model building of one subunit with icosahedral constraints maintained for all others within an asymmetric unit. In parallel with this process, real space averaging and solvent flattening was imposed.

A variety of Fourier syntheses were calculated using observed structure amplitudes, Fo, and Fo − Fc, where Fc were structure amplitudes calculated from the refined model in the relevant unit cell. For these syntheses, phases calculated from the model were used. Difference electron density maps with coefficients Fo − Fc, where Fo was experimentally determined by phase refinement techniques were also computed. A third type of difference electron density map was calculated by using phases from both, Fo and Fc, structure factors. These "vector difference maps" as they are termed were also used in some previous investigations (Tsuruta et al., 1998; Larson et al., 2005).

Refinement statistics for each crystal form are shown in Table 1. The model, originally derived from the $P4_232$ crystals (Ban and McPherson, 1995), was also refined further using CNS v.1.1. Readjustment of side-chain rotamers and inclusion of additional water molecules lowered the *R* factor to 17.9% using the same 1.9 Å resolution data as previously and structure

Table 1
Refinement statistics

Space group	$P2_13$	R3	$P4_232$
Unit cell dimensions (Å, °)	$a = b = c = 226.35$	$a = b = 175.47$ $c = 418.29$	$a = b = c = 183.0$
Z	4	3	2
Number of viral subunits per A.U.	20	20	5
Resolution range (Å)	20–3.3	50–4.6	30–1.9
Sigma cutoff	3.0	0.0	3.0
Number of reflections in working set	45,535	20,918	67,259
Total number of atoms from			
Protein	1,061	1,061	1,061
Solvent	0	0	98
R factor (%)	23.88	26.40	17.90
Average			
B-factor ($Å^2$)			
Protein	49.44	30.20	17.60
Solvent	–	–	33.56
RMS deviation			
Bonds (Å)	0.010	0.013	0.005
Angles (°)	1.519	1.870	1.502

amplitudes greater than 3.0 sigma. The SPMV model for the R3 unit cell, which had an asymmetric unit of one third of a particle, refined to an *R* of 26.4% using data in the resolution range 50 to 4.6 Å, with no cutoff on the data. The model in the $P2_13$ cubic unit cell, having the same asymmetric unit size, refined to an *R* of 23.9% using 20 to 3.3 Å data with a 3 sigma cutoff.

The change in diameter of the virion between the original $P4_232$ crystals at room temperature and the $P2_13$ crystal studied under cryogenic conditions was a contraction of only 0.42 Å. This is rather small considering the temperature difference and may even be due to the glutaraldehyde treatment carried out before freezing. The difference between the original virion model and that obtained from the R3 rhombohedral crystals, on the other hand, was substantial. The particle in the R3 unit cell exhibited an expansion of 6.96 Å, about 4% of the diameter. Because both of the $P4_232$ and R3 crystals were grown and analyzed at room temperature, and given the results with the $P2_13$ crystals above, we conclude that the size change is a consequence of the pH difference, which is basic for the R3 crystals and below neutral for the $P4_232$ crystals. There appears to be a structural transition, which occurs near neutrality that produces an overall swelling of the particle. This is not uncommon in small icosahedral viruses, and it has been observed in STMV (Kuznetsov et al., 2001), BMV (Lucas et al., 2002), and numerous others (Casjens, 1985). This transition has been suggested to play a role in the decapsidation of the virus, which must occur upon infection (Kaper, 1975), but there is no convincing evidence that this is so.

Fig. 2 shows the electrostatic surface of SPMV both inside and outside. The predominance of positive charge on the interior of the capsid is quite remarkable. It is a clear indication that the RNA is interacting with the coat proteins through its negatively charged phosphate backbone. The 16 amino acid long N-terminal polypeptide, which was not observed in the original structure determination, carries a total of seven basic residues and is almost certainly engaged with the encapsidated nucleic acid as well. The amino acid sequence of SPMV coat protein is as follows:

MAPKRSRRSN **RRAGSR**AAAT SLVYDTCYVT LTERATTSFQ RQSFPTLKGM GDRAFQVVAF
TIQGVSAAPL MYNARLYNPG DTDSVHATGV QLMGTVPRTV RLTPRVGQNN WFFGNTEEAE
TILAIDGLVS TKGANAPSNT VIVTGCFRLA PSELQSS

and the amino-terminal polypeptide is in boldface. In the case of STMV, the initial 15 amino acid residues were similarly ambiguous, but alternate paths for the polypeptide could be deduced from low-resolution difference electron density maps (Day et al., 2001).

Fig. 3 shows cross sections of SPMV particles in the R3, $P2_13$, and $P4_232$ unit cells with the averaged Fo maps represented in gray. The electron densities were calculated at 4.6 Å resolution, the protein section masked, and the remaining density contoured at 0.6 sigma. Although the detailed features of the density differ between the rhombohedral and the two cubic crystals, the gross density distribution inside the particle is consistent among the three crystal forms, and it can be considered in terms of two rings of density. The first, a highly concentrated band of density, extends about 20 Å from the interior surface of the protein capsid to the center. A disordered region is then followed by another ring of density. We feel it prudent at this point to comment only upon the band of density closest to the capsid. Three distinct features emerged from an inspection of the density just within the protein shell.

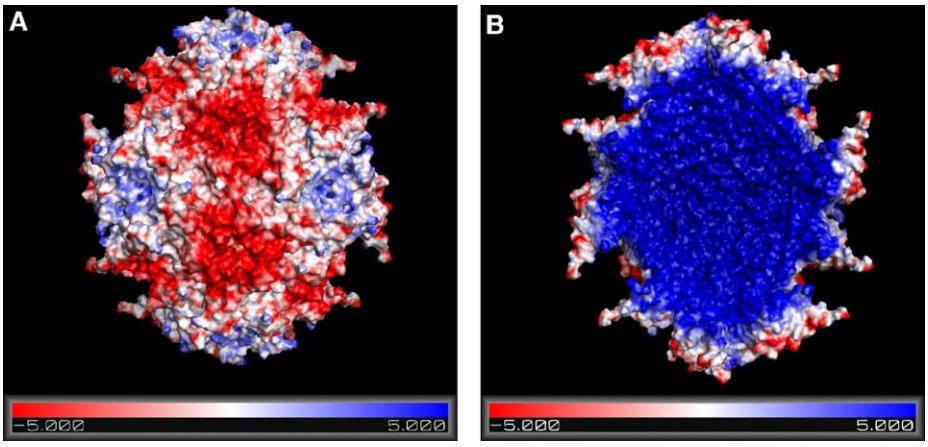

Fig. 2. Electrostatic surfaces showing 20 protein subunits that form the exterior (a) and interior (b) of the particle. Positively and negatively charged areas are represented in blue and red, respectively, at a kT level of 5. A dielectric constant of 4.0 was used for the protein and 80.0 for the solvent.

The amino-terminal polypeptide

Although the degree of disorder inside the particle is greater for SPMV than for STMV, clear indications of amino-terminal polypeptide density were found in the averaged native electron density maps calculated at low resolution, and using data from R3 crystals and their corresponding experimental phases. Less imposing indications of ordered polypeptide were also observed in equivalent maps based on the $P2_13$ and $P4_232$ crystals, although they indicated a slightly different path for the amino-terminus.

Viewed along an icosahedral twofold axis, the electron density inside the particle shows an unbroken chain of density near the axis. At 4.6 Å resolution, it might have been impossible to model this density had it not been that the first residue seen in the original 1.9 Å map (Ala 17) was perfectly contiguous with it, thereby creating a continuous strand of density, which extended from alanine 17 toward the center of the particle. It is therefore reasonable to conclude that the strand of density corresponds to part of the amino-terminal tail that was unobserved in the original structure determination. Addition of ten amino acid residues was straightforward and the resultant chain is illustrated in Fig. 4.

Corresponding electron density maps for both cubic crystals were not as unambiguous as for R3 unit cell electron density maps. They too showed extensions of the polypeptide inward at the twofold axis and away from alanine 17, but indicated a direction for the distal amino acid residues that deviated somewhat towards the fivefold axis.

RNA conformation

In STMV, clearly defined density for double helical RNA was observed centered on the twofold icosahedral axes. Because SPMV is also a small satellite plant virus, it might have been expected that its RNA would have a structure similar to that of STMV RNA. Electron density maps of SPMV show, however, that no duplex RNA is found at the same position as in STMV. On the contrary, amino-terminal polypeptides of SPMV in the R3 unit cell occupy the regions around the dyads. There was,

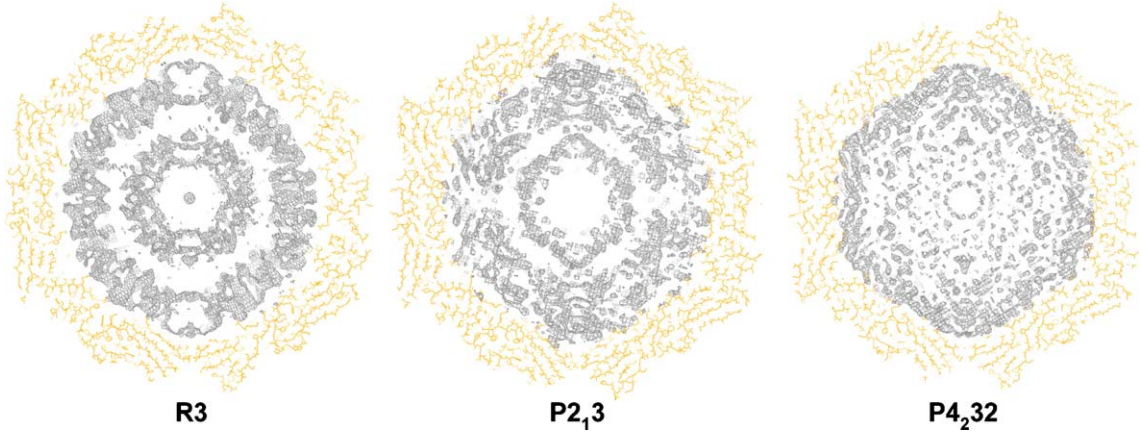

Fig. 3. The difference electron density in the interior of the SPMV particle as visualized for the three crystal forms is illustrated by averaged Fo maps using 4.6 Å data and contoured at 0.6 sigma. The fivefold axis is oriented along the orthogonal *y* axis and the twofold axis is along the orthogonal *x* axis.

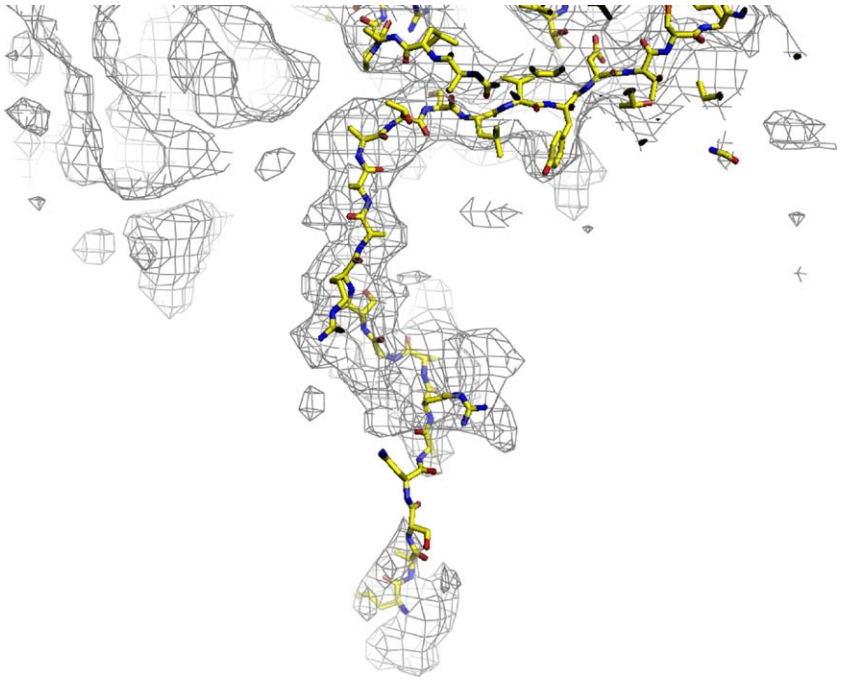

Fig. 4. The electron density map from the R3 crystal, shown here, was used to build an additional 10 amino-terminal residues. The new amino-terminal residue is Arg 7 and is located at radius 24 Å.

however, an indication of RNA in the neighborhood of the icosahedral fivefold axis. This was characterized by a distinctive mass of electron density clustered at about 60 Å radius from the center of the particle and virtually in contact with the interior surface of the capsid.

There is a high concentration of positively charged side chains at the interior surface of the protein pentamer (illustrated in detail in Ban and McPherson, 1995). A total of five symmetrical arginine residues are arranged within a circle of 21 Å diameter and interact closely with the density mass observed within the pentameric capsomere. A prominent feature of the electron density mass beneath the protein pentamer is a column of density having a diameter of 18–20 Å, aligned along the fivefold axis itself. The column of density is not unbroken, but is striated, or layered. That is, it exhibits an alternating series of strong and weak planes perpendicular to the fivefold axis, like rungs on a ladder in cross section. This is shown in Fig. 5.

The characteristic pattern of strong and weak bands along this column was seen in electron density maps for both the R3 and $P4_232$ crystal forms. The spacing of the bands, which is quite regular, is 3.2–3.5 Å, which is about what is expected for helical nucleic acids of the B form. Four to five RNA base pairs, as they would appear if parts of a helix, were readily fitted into the column of density. Similar striated columns of density, much like those seen here, were also found previously on the fivefold axes of another virus, TYMV (Larson et al., 2005), where they were interpreted as duplex RNA segments. Because the base pairs are close to perpendicular to the fivefold axes, even if they are fivefold rotationally disordered, the planes of density belonging to the base pairs persist.

Presumably, the duplex RNA is a short four or five base pair stem that is closed at its end by a loop that occupies the cavity within the pentameric capsomere. This is also what was seen in TYMV, although there, the loops were ordered and well resolved. As illustrated schematically in Fig. 6, the loops in SPMV are likely to be different sizes, have different conformations, and probably have arbitrary orientations. Thus, they would appear only as disordered density in Fourier maps, as we did indeed observe.

The single-stranded RNA

Around the threefold axis, directly beneath the capsid interior surface, there are distinct density masses, which are in close proximity to nine arginine side chains. Fig. 7 shows the interior surface of the capsid trimer and the distribution of the positively charged residues. An averaged Fo electron density map calculated with experimental phases with R3 unit cell diffraction data is shown in Fig. 7a. Two of the three major features of this density mass belong to the amino-terminal polypeptide, which tracks toward the center of the particle, and to the RNA found around the fivefold axis. Fig. 7b indicates their location. The quantity of density at the triad is comparable to that found at the five- and twofold axes. It appears unlikely that the remaining five amino-terminal residues could account for the density. Furthermore, it is far more probable that the RNA backbone rather than other positively charged amino acids are in close contact with the nine arginine

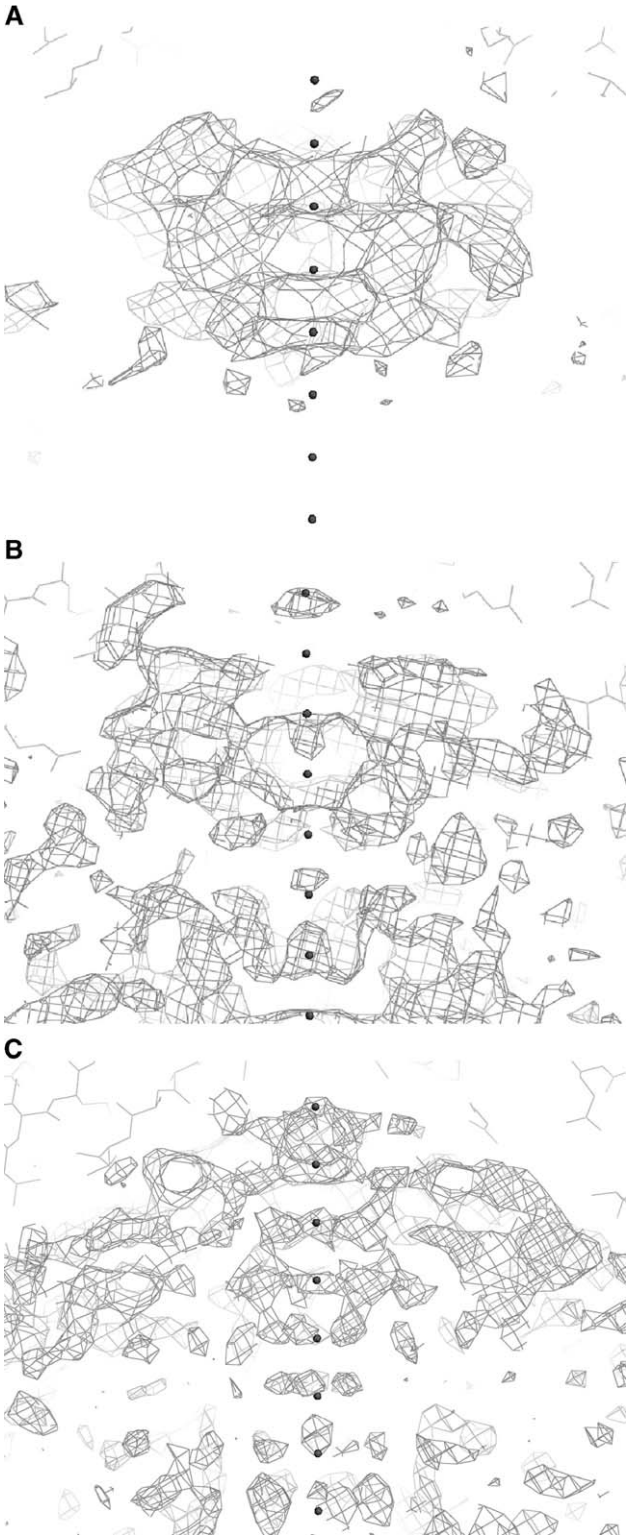

Fig. 5. Electron density maps viewed perpendicular to the fivefold axis in (a) R3, (b) $P2_13$, and (c) $P4_232$ crystals. Averaged Fo maps using experimentally determined phases were calculated at 4.6 Å and contoured at 1.8 sigma in the R3 crystal, and at 3.3 Å and contoured at 0.6 sigma in both cubic forms. The black balls are traced along the fivefold axis and equally spaced by 3.6 Å.

side chains. Although exhibiting no distinctive features of nucleic acid, the density connecting the triad and the pentamer likely belongs to single-stranded RNA. Electron density masses at the three- and fivefold axes clearly connect through passages stemming from either "branch". This density distribution was not as clearly evident in corresponding Fourier maps from cubic crystals, even with truncation of phases at 4.6 Å.

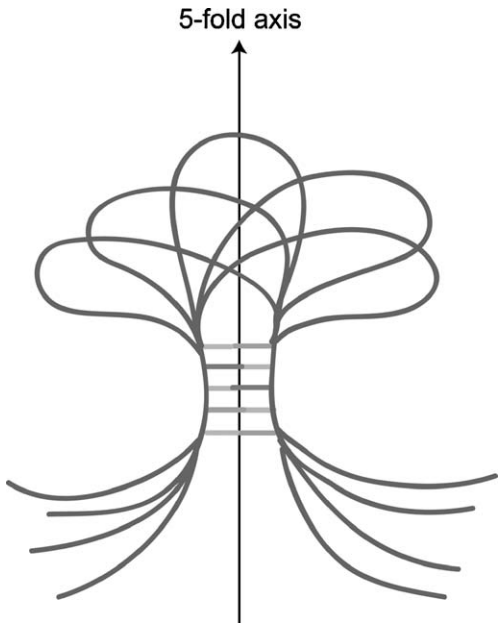

Fig. 6. Example of disordered stem–loops at the fivefold icosahedral symmetry axis. The latitudinal base stacking distribution coincides independent of the stem–loop orientation. Contributions to the structure factors from this type of structure will be principally from the ordered and overlapped regions.

Fig. 8 shows the interior surface of the SPMV capsid as seen in the R3 unit cell asymmetric unit, which is comprised of 20 protein subunits. In this figure, the additional 10 amino-terminal residues are shown. Positively charged side chains are indicated in blue. The positively charged side chains at the inner surface of SPMV are exclusively arginines. A total of three per protein subunit directly face the density inside the particle. As in STMV, no lysine residues were involved, suggesting arginine to be the preferred amino acid for such nonspecific protein–RNA interactions. Indeed, in SPMV, the amino-terminal polypeptide is constituted of 6 arginines and only 1 lysine residue.

RNA packing in the virion

The placement of the additional 10 amino-terminal residues of the coat protein subunits (600 total amino acids within the virion) has significant consequences for the disposition of the encapsidated nucleic acid. Sixty polypeptides protrude into the interior of the virion for a distance of about 30 Å where the course of the chain is then lost. At 25 Å radius, there need still be space to accommodate the final five residues of each polypeptide, a total of 300 amino acid residues. These final residues probably account for the band of strong electron density seen in Fourier maps that is centered at 25 Å radius.

The effect of the invading polypeptides is to partition the space within the virion into discrete chambers between radius 25 Å and the interior surface of the capsid. This is illustrated in Fig. 9. There are rather large chambers beneath the pentameric capsomeres, and smaller passages at the threefold axes that provide interconnection. The RNA can only occupy space that is not occupied by the protein. Indeed, the most prominent masses of density observed in the Fourier maps, aside from the amino-terminal tails, fill the fivefold and threefold chambers, as described above.

The protein provides a negative relief image of the space available to the nucleic acid inside the virion. From this, it appears that the RNA probably has the tertiary conformation of a series of density masses, disposed within the fivefold cavities, connected by more extended polynucleotide chain passing through the smaller cavities at the threefold axes. This is compatible with a linear distribution of clusters of secondary structural elements of RNA, as previously proposed for several other small icosahedral viruses (Kuznetsov et al., 2005; Larson and McPherson, 2001; Larson et al., 2005).

Discussion

It seems evident from this analysis that the two satellite viruses SPMV and STMV are different in the way in which single-stranded RNA is organized inside the virion, and the why by which the RNA interacts with the interior surface of the capsid. In both viruses, the interactions are principally electrostatic, mediated by arginines bound nonspecifically to the polyphosphate backbone of the nucleic acid. On the other hand, STMV RNA has stem–loop secondary structural elements disposed at every icosahedral dyad, with the helical stem positioned symmetrically in a cradle formed by capsid protein dimers. SPMV does not. In SPMV, the RNA appears to be organized in rather discrete chambers at the

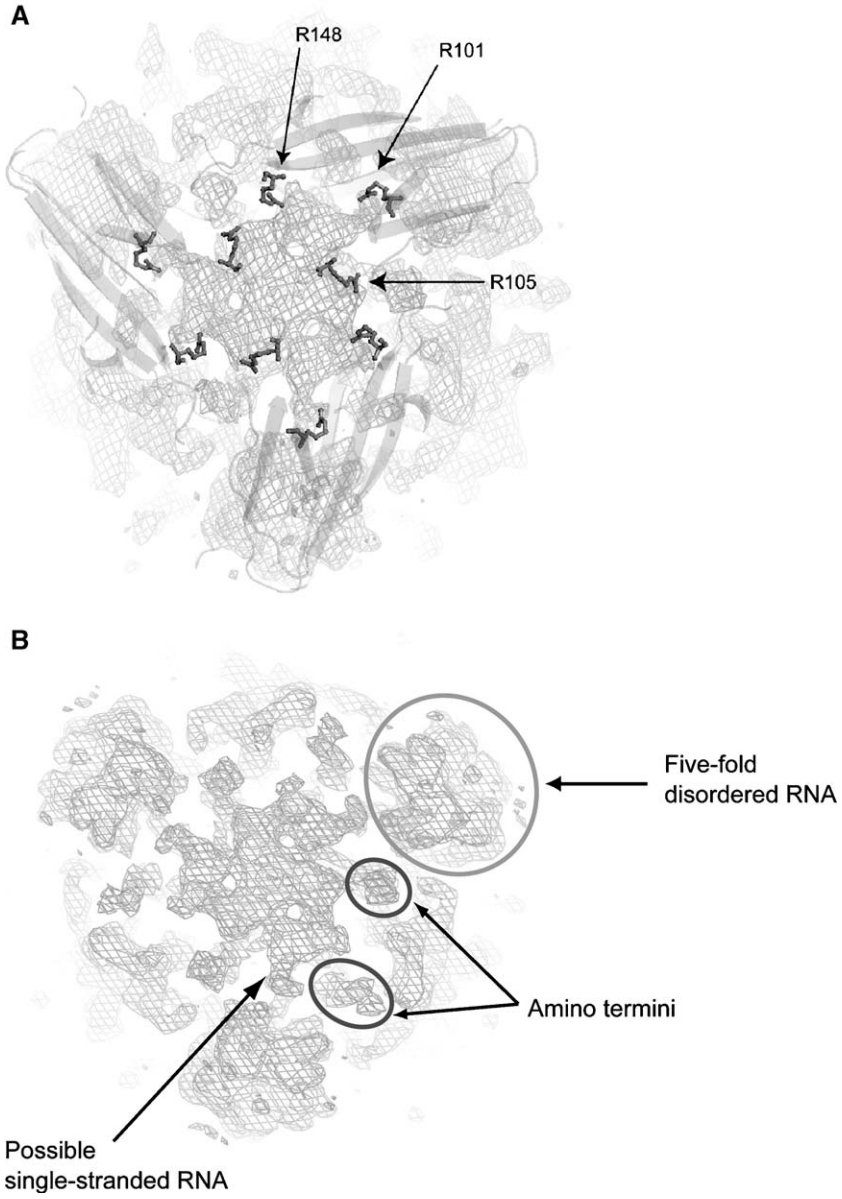

Fig. 7. Schematic diagram identifying the locations of nine arginine side chains that closely interact with distinctive masses of electron density inside the SPMV particle in the R3 crystal. (a) Arginines number 148, 101, and 105 make close contacts with density around the threefold axis. (b) An averaged Fo map using experimental phases was calculated to 4.6 Å and contoured at 1.2 sigma after masking out the protein contribution.

fivefold axes, interconnected through passages crossing near the threefold axes. The interior space at the dyads, occupied by RNA in STMV, is in SPMV occupied by the amino-terminal polypeptides. Within the pentameric chambers, at least one short segment of double helical RNA of four to five base pairs is aligned, at least approximately, along the fivefold axis. Though fivefold disordered, it is still recognizable, principally by the ladder of base pairs of constant spacing.

In both STMV and SPMV, the distribution of RNA inside the virus is compatible with an RNA molecule existing as a linear sequence of secondary structural domains, stem–loops in the case of STMV, probably a more irregular and complicated ensemble for SPMV, distributed along its length. In STMV there are likely 30 stem–loops (at each dyad), whereas in SPMV there are likely to be 12 similar sized groupings of more elaborate configurations of stems, loops, and extended RNA chain.

SPMV represents a second observation of helical RNA aligned along, or approximately along icosahedral fivefold axes. Thus, we have now identified in small icosahedral viruses a number of common motifs. The secondary structural elements are visible by X-ray crystallography, though they are partially disordered, because they display approximate, or pseudosymmetry elements that are consistent with icosahedral symmetry elements. Among these are helical segments positioned perpendicular to icosahedral twofold axes, and duplex elements aligned along fivefold axes. Other motifs have also been observed, such as the trefoil of RNA at the threefold axes of cowpea chlorotic mosaic virus (Speir et al., 1995), and the

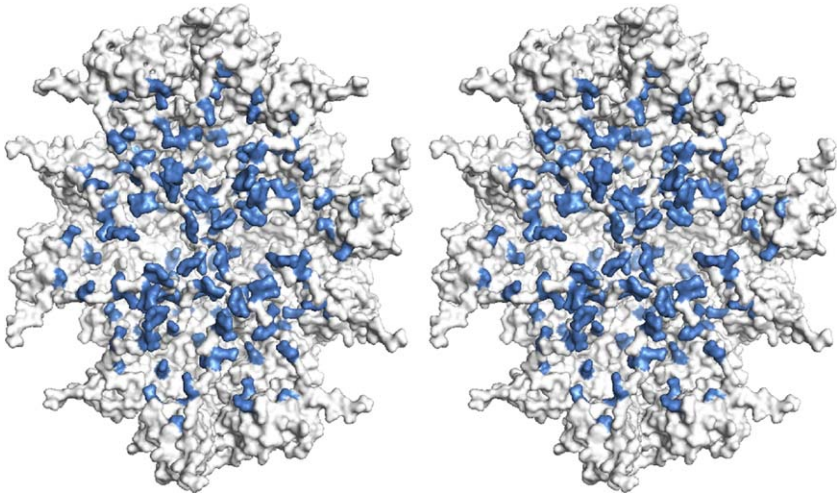

Fig. 8. Stereo view of the surface representation of the interior of the SPMV capsid. This model corresponds to the asymmetric unit of the R3 crystal. Positively charged side chains are highlighted in blue.

symmetrically disposed invasive loops within the capsomeres of TYMV (Larson et al., 2005).

The only reasonable assembly mechanism for SPMV, and very likely STMV as well, is a coordinated, cooperative condensation of the coat protein and the RNA, simultaneously involving both kinds of molecules. This appears the only mechanism compatible with the conformations of the RNA from small icosahedral viruses observed by AFM (Kuznetsov et al., 2005) and the dynamics of that RNA. It is also compatible with assembly through an initially disordered aggregate of RNA and protein that has some of the properties of a micellar structure (McPherson, 2005).

It seems clear from the intricate partitioning of the interior volume by the amino-terminal strands, the deep penetration of the amino-terminal polypeptides into the central mass of the RNA, and the encapsidation of the RNA in a series of interconnected chambers, that certain mechanisms for encapsidation of the RNA can be ruled out. It appears almost inconceivable that the RNA first folds into its ultimate, encapsidated conformation and that the capsid protein then coats its surface to form an icosahedron. There would simply be no reasonable way for the amino-terminal polypeptides (16 amino acids, 50 Å in length if fully extended) to penetrate the mass of RNA and invest the interior, as we observe to be the case with SPMV. It seems similarly unlikely that the coat protein would form a partially or nearly completely constructed icosahedral capsid and then draw the RNA inside and arrange it in an intricate series of chambers at the fivefold axes.

The results here lend further support to the observations and conclusions that virions swell or contract in response to alterations in their physical and chemical environment. Such changes, as long suspected, do include changes in the conformation of the RNA, and possibly the amino-terminal polypeptides, and the degree of icosahedrally consistent order within the virion. Thus, we continue to believe that investigation of the same virus in different crystal forms, grown under different conditions of ionic strength and pH, may provide a way to obtain at least a glimpse of the arrangement of RNA inside some viruses.

The question remains as to how the SPMV protein shell can encapsidate the PMV satellite RNA. Presumably, the capsid is essentially the same icosahedral shell as for the native particle, as that architecture is embedded in the structure of the coat protein subunits. One possibility is that the SPMV capsid requires the RNA only to nucleate assembly of the capsid and that construction can begin around any strand of RNA of almost any size that does not exceed the capacity of the virion. This, however, would leave the interior of the capsid mostly empty and the many positively charged amino acids unneutralized. The satellite RNA is only 350 nucleotides in length, which would be about half the normal complement of the native particle.

On the other hand, two copies of the satellite RNA would make a nearly complete complement for the virion. At this time, it is not clear if one or more copies of the satellite RNA are in fact encapsidated in a single particle. If, indeed, a cooperative condensation involving both protein and RNA is responsible for SPMV assembly, where the formation of the protein shell effectively marshals the RNA into a particular arrangement, then involvement of multiple strands of nucleic acid would be entirely plausible.

Indeed, there are numerous examples in the literature of a single virus particle encapsidating multiple RNA molecules, turnip yellow mosaic virus and brome mosaic virus are but two examples (Kaper, 1975). Precisely how this comes about, however, is not well understood.

Materials and methods

SPMV was purified from virus-infected leaves of white pearl millet grown in a temperature-controlled greenhouse. The satellite virus was separated from PMV by differential precipitation with PEG 8,000 and NaCl as previously described (Day et al., 1994). In general, yields were of the order of 10 mg per 100 g of leaves. Using a variety of

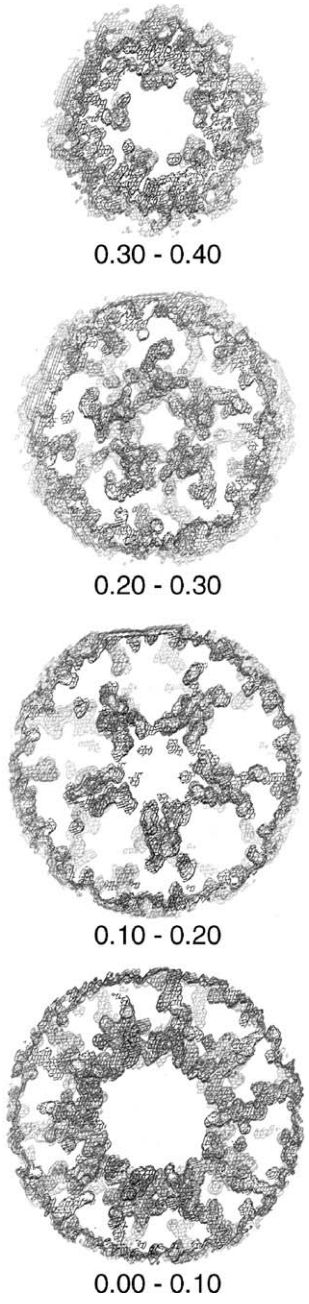

Fig. 9. A mask was drawn about the protein atoms of SPMV, including the added amino-terminal polypeptide residues, at 2.0 Å distance from their centers, to delineate the boundary between protein and the space available for accommodation of nucleic acid. The interior volume is here presented as four contiguous cross sections through a hemisphere of the particle between the center of the virion (at $z = 0.00$) and the interior surface of the capsid (at about $z = 0.40$). The RNA must be distributed among the discrete chambers at the fivefold vertices of the icosahedron and connected through passages at the threefold axes.

commercially available crystallization screens (Hampton Research, Aliso Viejo, CA), a number of conditions were obtained which yielded crystals having unique morphologies. The crystallization conditions were optimized (McPherson, 1999) by incremental variation of relevant parameters such as salt, PEG concentrations, pH, temperature, and other ion concentrations.

Crystals were grown for X-ray analysis by sitting drop vapor diffusion using Cryschem plates (Hampton Research) with 6 μl droplets composed of 1:1 ratios of stock virus solution (12 mg/ml) with the reservoir solution. All of the crystal forms but one were grown at pH from 5 to 7, and from PEG 3350 at concentrations ranging from 6% to 14%. The lone exception was a rhombohedral crystal form, which was also grown from 6% to 8% PEG 3350, but at pH between 8 and 9.

The characteristics of the new crystallographic unit cells were established by X-ray diffraction. The analyses were performed using an R-axis IV image plate detector system and a Rigaku RU-200 generator fitted with Osmic mirrors (Rigaku Corp., Woodland, TX). Three-dimensional X-ray diffraction data were also collected on beamline 5.0.1 at the Advanced Light Source at the Lawrence-Berkeley Laboratories in Berkeley, CA, using crystals that were cryogenically frozen. Data were collected on crystals at room temperature using the R-axis system. The rotation angles were 0.5°–0.75° with exposure times, dependent on the particular crystal, of 30 s at ALS, and 4–6 min on the R-axis system. The data collection statistics for the three new crystal forms, calculated using D*TREK (Pflugrath, 1999) and HKL2000 (Otwinowski and Minor, 1997), are shown in Table 2.

The orientations and positions of the virus particles in the unit cells were determined using molecular replacement techniques based on the model earlier derived from the cubic crystals of space group $P4_232$ (Ban and McPherson, 1995). Particle orientations were defined by self-rotation functions calculated with the program GLRF (Tong and Rossmann, 1997) and CNS v.1.1 (Brünger et al., 1998). Rotation matrices and position vectors were assessed manually using the program X-PLOR (Brünger, 1992). Strict noncrystallographic symmetry together with skew matrix and vector were then applied to further refine a single subunit. Once refinement converged, solvent flattening and NCS averaging were used to refine calculated structure amplitudes against observed diffraction data. Rigid body, simulated annealing, Powell minimization, and B-factor refinements were carried out using CNS v.1.1 (Brünger et al., 1998) with bulk solvent corrections for scaling of low-resolution structure amplitudes. Models for all crystal forms were built and

Table 2
Data processing statistics

Space group	$P2_13$	R3	P4
Unit cell dimensions (Å)	$a = b = c = 226.35$	$a = b = 175.47$ $c = 418.29$	$a = b = 167.06$ $c = 473.21$
Number of viral particle per unit cell	4	3	4
Resolution range (Å)	100.0–3.3 (3.36–3.30)	50.0–4.6 (4.76–4.60)	100.0–4.0 (4.07–4.00)
Observed reflections	5,541,624	150,691	1,381,373
Unique reflections	58,624 (2,892)	25,998 (2,564)	101,045 (5,241)
R sym (%)	12.3 (44.0)	16.7 (46.2)	14.0 (46.4)
I/sigma	27.7 (6.5)	5.8 (2.0)	7.8 (2.2)
Completeness (%)	100.0 (100.0)	97.4 (95.4)	90.0 (94.0)

Values in parentheses are for the highest resolution shell.
$R - \text{sym} = \sum(|I - \langle I \rangle|)/\sum I$.

adjusted with the program O v8.0 (Jones et al., 1991) and images were generated using PyMol (DeLano, 2002).

Acknowledgments

This research was supported by a grant from the NIH (GM58868-02). D. Makino was supported by CNPq (Conselho Nacional de Desenvolvimento Científico e Tecnológico), an entity of the Brazilian government for the development of science and technology. The authors wish to thank Mr. Aaron Greenwood for assistance in preparation of figures.

References

Ban, N., McPherson, A., 1995. The structure of satellite panicum mosaic virus at 1.9 Å resolution. Nat. Struct. Biol. 2, 882–890.

Ban, N., Larson, S.B., McPherson, A., 1995. Structural comparison of the plant satellite viruses. Virology 214, 571–583.

Brünger, A.T., 1992. X-PLOR A System for X-ray Crystallography and NMR, Version 3.1. Yale University, New Haven and London.

Brünger, A.T., Adam, P.D., Clore, G.M., DeLano, W.L., Gros, P., Grosse-Kunstleve, R.W., Jiang, J.-S., Kuszewski, J., Nilges, M., Pannu, N.S., Read, R.J., Rice, L.M., Simonson, T., Warren, G.L., 1998. Crystallography and NMR system: a new software suite for macromolecular structure determination. Acta Cryst. D54, 905–921.

Buzen Jr., F.G., Niblett, C.L., Hooper, G.R., Hubbard, J., Newman, M.A., 1984. Further characterization of panicum mosaic virus and its associated satellite virus. Phytopathology 74, 313–318.

Casjens, S., 1985. The Structure and Assembly of Viruses. Jones and Bartlett Inc, Boston, MA.

Day, J., Ban, N., Patel, S., Larson, S.B., McPherson, A., 1994. Characterization of crystals of satellite panicum mosaic virus. J Mol Biol. 238, 849–851.

Day, J., Kuznetsov, Yu. G., Larson, S.B., Greenwood, A., McPherson, A., 2001. Biophysical studies on the RNA cores of satellite tobacco mosaic virus. Biophys. J. 80, 2364–2371.

DeLano, W.L., 2002. The PYMOL Molecular Graphics System. DeLano Scientific, San Carlos, CA.

Desvoyes, B., Scholthof, K.B., 2000. RNA: protein interactions associated with satellites of panicum mosaic virus. FEBS Lett. 485, 25–28.

Francki, R.I.B., 2005. The viruses and their taxonomy. The Plant Viruses, v.1, Polyhedral Virions with Tripartite Genomes. Plenum Press, New York, pp. 571–607.

Gasteiger, E., Hoogland, C., Gattiker, A., Duvaud, S., Wilkins, M.R., Appel, R.D., Bairoch, A., 2005. Protein Identification and Analysis Tools on the ExPASy Server. In: Walker, John M. (Ed.), The Proteomics Protocols Handbook. Humana Press, pp. 571–607.

Jones, T.A., Liljas, L., 1984. Structure of satellite tobacco necrosis virus after crystallographic refinement at 2.5 Å resolution. J. Mol. Biol. 177, 735–767.

Jones, T.A., Zou, J.Y., Cowan, S.W., Kjeldgaard, M., 1991. Improved methods for building protein models in electron density maps and the location of errors in these models. Acta Cryst. A47, 110–119.

Kaper, J.M., 1975. In: Neuberger, A., Tatum, E.L. (Eds.), The Chemical Basis of Virus Structure, Dissociation and Reassembly, Frontiers of Biology. North-Holland Publishing Company, Amsterdam.

Kuznetsov, Yu. G., Larson, S.B., Day, J., Greenwood, A., McPherson, A., 2001. Structural transitions of satellite tobacco mosaic virus particles. Virology 284, 223–234.

Kuznetsov, Yu. G., Daijago, S., Zhou, J., Semler, B.L., McPherson, A., 2005. Atomic force microscopy analysis of icosahedral virus RNA. J. Mol. Biol. 347, 41–52.

Larson, S.B., McPherson, A., 2001. Satellite tobacco mosaic virus RNA: structure and implications for assembly. Curr. Opin. Struct. Biol. 11, 59–65.

Larson, S.B., Koszelak, S., Day, J., Greenwood, A., Dodds, J.A., McPherson, A., 1993. Double-helical RNA in satellite tobacco mosaic virus. Nature 361, 179–182.

Larson, S.B., Lucas, R.W., Greenwood, A., McPherson, A., 2005. The RNA of turnip yellow mosaic virus exhibits icosahedral order. Virology 334, 245–254.

Lucas, R.W., Larson, S.B., Pherson, A., 2002. The crystallographic structure of brome mosaic virus. J. Mol. Biol. 317, 95–108.

Masuta, C., Zuidema, D., Hunter, B.G., Heaton, L.A., Sopher, D.S., Jackson, A.O., 1987. Analysis of the genome of satellite panicum mosaic virus. Virology 159, 329–338.

McPherson, A., 2005. Micelle formation and crystallization as paradigms for virus assembly. Bioessays 27, 447–458.

Otwinowski, Z., Minor, W., 1997. Processing of X-ray Diffraction Data Collected in Oscillation Mode. Methods Enzymol. 276, 307–326.

Pflugrath, J.W., 1999. The finer things in X-ray diffraction data collection. Acta Crystallogr. D55, 1718–1725.

Scholthof, K.-B.G., 1999. A synergism induced by satellite panicum mosaic virus. Mol. Plant-Microb. Interact. 12, 163–166.

Speir, J.A., Munshi, S., Wang, G., Baker, T.S., Johnson, J.E., 1995. Structures of the native and swollen forms of cowpea chlorotic mottle virus determined by X-ray crystallography and cryo-electron microscopy. Structure 3, 63–78.

Tong, L., Rossmann, M.G., 1997. Rotation function calculations with GLRF program. Methods Enzymol. 276, 594–611.

Tsuruta, H., Reddy, V., Wikoff, W., Johnson, J.E., 1998. Imaging RNA and dynamic protein segments with low resolution virus crystallography: experimental design, data processing and implications of electron density maps. J. Mol. Biol. 284, 1439–1452.